Fuel 366 (2024) 131337

Contents lists available at ScienceDirect

Fuel

journal homepage: www.elsevier.com/locate/fuel

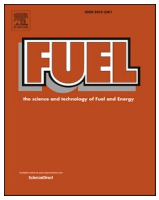

Full Length Article

3D shape and size characterization of micron-sized coal particle with XRCT and SH

Qiwen Jin [a,b], Zhiming Lin [a], Yingchun Wu [a], Xuecheng Wu [a,b,*]

[a] State Key Laboratory of Clean Energy Utilization, Zhejiang University, Hangzhou 310027, China
[b] Key Laboratory of Clean Energy and Carbon Neutrality of Zhejiang Province, Zhejiang University, Hangzhou 310027, China

ARTICLE INFO

Keywords:
Fuel particle
Morphology characterization
Particle size
X-ray computer tomography
Spherical harmonics

ABSTRACT

The shape and size of solid fuel particles are significant parameters in combustion process, and have attracted broad attentions in simulation and experiment studies. In this study, X-ray computer tomography (XRCT) and spherical harmonics (SH) were introduced and combined to conduct accurate morphology characterization of micron-sized coal powder in three dimensions (3D) with purpose of providing references for morphology characterization, size measurement, and modeling of solid fuel particles. The shape parameters including volume, surface area, sphericity index, specific surface area, enlongation index, and flatness index, and the size parameters including diameter of volume equivalent sphere, three principal dimensions, and sieve size, were obtained with SH expansion. Validation on standard geometries demonstrated the accuracy of the method under the SH degree $N \geq 20$, with errors for volume, surface area, and sieve size within 1 %, 3 %, and 2.5 %, respectively. These parameters were analyzed statistically to reveal the morphological characteristics of micron-sized coal powder. The Zingg diagram indicated that nearly 60 % of the coal powder particles are nearly spherical. Comparison among 3D size, 2D size, and sieve size implied that characterizing with 2D size may overestimate the fineness of coal powder. Although there was a variance in the particle size distribution, it was demonstrated that there exists a strong linear relationship between the 3D size, 2D size, and sieve size. The method could serve as a functional auxiliary tool for fuel particle research.

1. Introduction

Solid fuels, including coal, biomass, and metal, are dominant energy and material sources in various industrial fields and have attracted broad attentions. Direct combustion after conversion to fine powder or coarse particles is one of the most common utilization of solid fuels. The morphological feature of fuel particle plays a critical role on combustion process as it influences the heat and mass transfer rate and reaction surfaces [1]. Numerous simulations [2–4] and experiments [5–9] have been conducted to study the particle shape effects on combustion characteristics of single fuel particle or particle clouds. In numerical investigations, fuel particles are generally assumed to be spherical [3]. Particle shape factor, defined as the ratio of the surface area of an equal-volume sphere to the actual surface area of the non-spherical particle, has been introduced by Backreedy et.al [10] to allow for the effects of irregular shape. Some studies used regular geometries such as cylinder, ellipsoid, and disc to represent fuel particles. Bonefacic et.al [4] have established a cylindrical particle model in pulverized coal and biomass co-firing process, with a better agreement with the experimental data than the existing sphere-based models. However, as for experimental investigations, fuel particles are qualitatively classified to near-spherical and irregular shapes [6,9] by using scanning electron microscope (SEM) or two-dimensional (2D) imaging methods. Due to the lack of complete three-dimensional (3D) morphology information, quantitative investigations of particle shape effects become a challenge. Schiemann et. al [5] have studied the impact of particle shape on the char burning by imaging pyrometry, and proposed that 3D particle shape measurement should be adopted for a more reliable analysis. Along with combustion, particle shapes of solid fuels also influence the flow characteristics in the isotropic turbulent flow [11] and pneumatic conveying [12].

Fuel particle size and particle size distribution (PSD) are significant parameters that are related to particle shape. Due to the irregularity, obvious disagreements in particle size distributions using different measurement techniques have been observed [13,14], as many techniques rely on spherical assumption. A range of methods have been utilized to measure PSD of fuel particles, including mechanical sieve,

* Corresponding author.
E-mail address: wuxch@zju.edu.cn (X. Wu).

https://doi.org/10.1016/j.fuel.2024.131337
Received 2 December 2023; Received in revised form 9 February 2024; Accepted 24 February 2024
Available online 10 March 2024

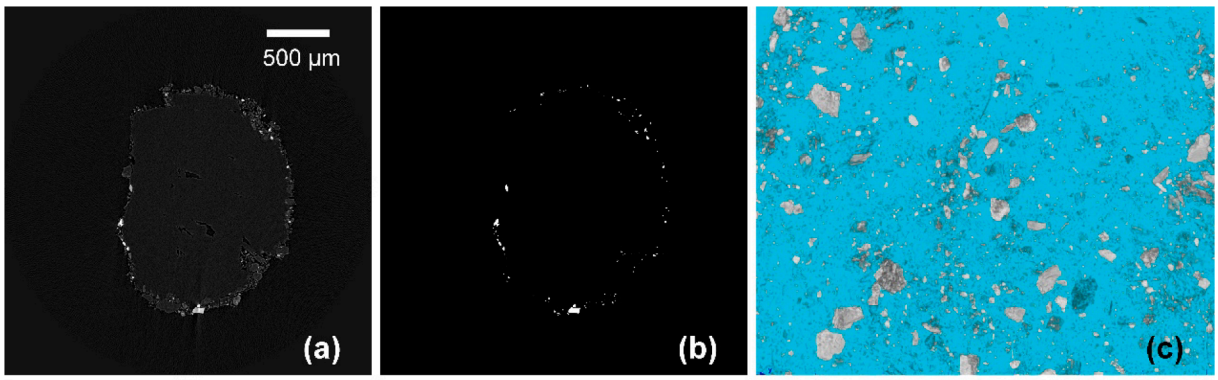

Fig. 1. Image processing of CT data. (a) Gray-scale slice image. (b) Binarized and segmented image. (c) 3D viewing of a local region.

dynamic image analysis, digital holography, and light scattering. Mechanical sieve, with advantages of low cost and simple operation, is the most used method for particle size analysis. In many studies investigating the effect of particle size, mechanical sieving is commonly employed to divide fuel particles into samples of different particle size grades. Mechanical sieving determines the minimum sieve aperture through which particles can pass. For a specific individual particle, this represents a unique characteristic size. Dynamic imaging and holographic imaging, on the other hand, calculate particle size information by recording the two-dimensional projections of particles and utilizing image processing algorithms. Based on particle morphology information, multiple characteristic particle sizes can be derived. The light scattering method measures the particle size of spherical particles that have an equivalent optical effect to the measured particles. Therefore, particle shape has a certain influence on the measurement results. The variability in these measurement results adds to the challenge of accurately characterizing the particle size distribution of fuel particles. Gil et al. [15] characterized the stand sieving method through image processing for milled biomass particles and their results showed that sieve size corresponded mostly with particle width. Trubetskaya et al. [16] compared four methods for PSD measurement of biomass particles, including 2D dynamic imaging analysis, light microscopy, laser diffraction, focused beam reflectance measurement, and sieving. They found that the sieving results were in agreement with the 2D dynamic imaging which was considered to be the most convenient characterization method, providing additional information on particle shape, whereas the laser diffraction and the focused beam reflectance measurement represented a significant disparity. Igathinathane and Ulusoy [17–19] have conducted an in-depth investigation on milled coal PSD characterization using machine vision, considering the mill type, coal type, and PSD model effects. Yang et al. [20] used ellipsoid model to process millimeter-size coal fragments and obtain PSD, aiming to provide a fast and precise method. Jin et al. [21] developed a digital holographic system for on-line pulverized coal fineness measurement and the maximum inscribed circle diameter was recommended to estimate the sieve size. It can be summarized from these existing studies that, researchers currently extensively investigate the shape and size characteristics of fuel particles based on two-dimensional image features, but there is a lack of research on the complete three-dimensional morphology of fuel particles. Corrections for differences in particle size representation due to particle irregularities (e.g., converting image results into sieving results) are typically obtained empirically through statistical data, and there is a lack of in-depth research into the relationships between different characteristic particle sizes of individual particles.

Thus, quantifying the 3D morphology of fuel particles could be conducive to further investigations on physical and chemical characteristics, e.g., more accurate shape and size characterization. Common methods for measuring the three-dimensional morphology of particles include multi-viewpoint imaging, laser scanning, and X-ray computed tomography (XRCT). Botlhoko et al. [22] used a three-dimensional tomography system with seven viewpoints to measure the volume of coal particles, combined with mass weighing to obtain particle density, thus evaluating their washability. However, this tomography method may overlook some surface concave details, leading to errors. Yang et al. [23] used a three-dimensional scanner to obtain three-dimensional models of anthracite coal particles and gangue particles, and they analyzed the three-dimensional morphological parameters. It is worth noting that the two methods mentioned are suitable for millimeter-sized large particles, and they face significant challenges when it comes to three-dimensional characterization of micron-sized small particles. Due to the powerful penetrating ability of X-rays, XRCT can provide information about the internal and external morphology of materials with resolutions reaching the micrometer or even nanometer level, which is far superior to techniques like laser 3D scanning [24]. XRCT has found widespread applications in particle morphology characterization in various fields such as geomechanics [25–27], construction materials [28,29], and additive manufacturing [30]. However, it has seen limited use in the characterization of micron-sized fuel particles. Spherical harmonic (SH) is a powerful method for characterizing the three-dimensional morphology of particles, featuring with compact representation, mathematical rigor, rotation invariance, and scalability. By converting three-dimensional point cloud data of an object into spherical harmonic coefficients, these coefficients encapsulate rich information about the object size and shape. Furthermore, spherical harmonic coefficients can be conveniently used to generate virtual particle models of specific shapes [31], which can be employed in simulation studies and other research applications [32].

The aim of this work is to perform comprehensive 3D shape and size quantification of fuel particles using XRCT and SH. Micron-sized coal powder obtained from a coal-fired power plant was taken as a research object. We firstly introduced sample preparation and 3D point cloud acquisition and processing. Then the basic theory and critical reconstruction procedures including parameterization and expansion of SH were introduced. Quantified calculation of 3D particle morphological properties and sizes with SH analysis was demonstrated. An algorithm was proposed to determine the particle sieve size based on the rotation invariance of SH. The method was verified by reconstructing several standard geometries. The 3D morphology and size of the coal sample were reconstructed and analyzed. This study proved that fuel particle characterization with XRCT and SH is feasible.

2. Materials and 3D data acquisition

2.1. Coal sample preparation

The micron-sized bituminous coal powder sample used in this study was obtained from the coal bunker of ball mill pulverizing system in a

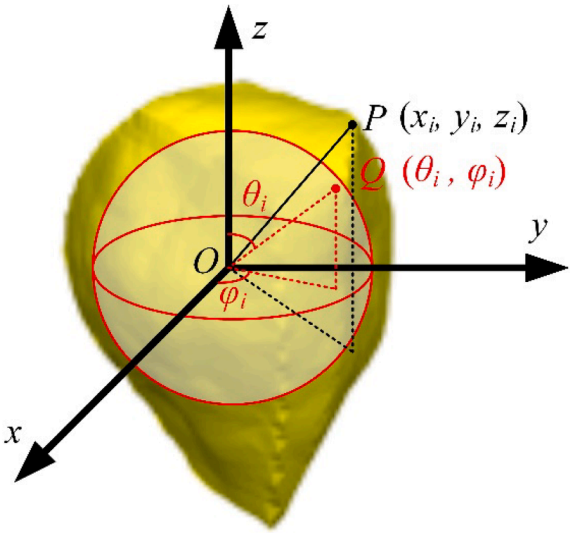

Fig. 2. Mapping of surface points on particles to the unit sphere.

thermal power plant. The coal sample was first dried over a stove to avoid particle agglomeration. When preparing the sample for XRCT, particle population that can be measured is expected to be as much as possible while particle movement to be minimized. Thus the dried sample were placed on a block of wax, making coal powder adhering on the wax in the rolling process.

2.2. 3D data acquisition with XRCT

XRCT was utilized to obtain 3D point cloud data of the coal powder. XRCT is capable of reconstructing internal and external morphological information of materials, with a high resolution down to sub-micro size, due to the strong penetrability of X-ray. The basic process of XRCT includes X-ray transmission and absorption, collection of projection data, and back projection and reconstruction. A series of 2D ray pictures are recorded at various scanning angles, generally by rotating the object. Then the ray pictures are converted to section images with numerical reconstruction algorithm. One can retrieve 3D image from these sections.

It is worth noting that XRCT is based on the differential absorption of X-rays by materials with different densities. Therefore, this method is applicable to different types of coal, requiring only a significant density contrast between the material under test and the surrounding medium to obtain high-quality 3D voxel data.

Bruker SkyScan2211, a nano/micro-CT scanning system, was used in this study, with voxel size of 1 μm × 1 μm × 1 μm. The reconstructed section images were stacked into a 3D matrix, which contains detailed structural information of the coal sample. Fig. 1(a) shows one gray-scale section image in which density difference between air, wax, and coal lead to the brightness and darkness. Then the gray-scale images were binarized to extract coal powder, as shown in Fig. 1 (b). Fig. 1 (c) shows some 3D particles of a local region. Small particles, with voxel number less than 512, were deleted to guarantee sufficient surface point for spherical harmonics reconstruction, whilst clean up the unexpected voxel noises. Thus, only particles with diameter larger than about 10 μm would be analyzed.

Furthermore, particles that do not constitute Genus-0 closed surfaces should be omitted, as they cannot be parameterized using spherical harmonics. A Genus-0 surface can be justified by the relation of vertex quantity and face quantity after meshing, conforming the formula

$$K_v - 0.5K_f = 2, \tag{1}$$

where K_v is the number of vertexes and K_f is the number of faces. Non Genus-0 particles may have complex topology, such as torus. Generally, pulverized particles are considered to be Genus-0. Hence, in this study, a few non Genus-0 coal powder were removed before spherical harmonics analysis.

3. Spherical harmonics for particle characterization

3.1. Basic theory

The spherical harmonics are a set of special functions defined on the surface of a sphere, which form a complete set of orthogonal functions, an orthonormal basis in other words. Therefore, any function defined on the surface of a sphere can be represented as a series of spherical harmonics. The spherical harmonics can also be regarded as the 3D extension of Fourier description method, suitable for modeling the 3D surface. One is able to reconstruct and analyze particle morphology after obtaining 3D point cloud data by XRCT or laser scan techniques.

Any surface defined in the spherical coordinates (denoted by $f : S^2 \rightarrow R$) can be expanded to spherical harmonics functions

$$f(\theta,\varphi) = \sum_{n=0}^{\infty}\sum_{m=-n}^{n} a_n^m Y_n^m(\theta,\varphi), \tag{2}$$

where $f(\theta,\varphi)$ represents the points coordinates in the surface, determined by the polar angles θ and azimuthal angles φ with ($\theta \in [0,\pi]$,$\varphi \in [0,2\pi]$). $f(\theta,\varphi)$ can be the Polar coordinates $r(\theta,\varphi)$ or Cartesian coordinates $(x(\theta,\varphi), y(\theta,\varphi), z(\theta,\varphi))^T$. $Y_n^m(\theta,\varphi)$ is the spherical harmonics function with degree n and order m. a_n^m is the corresponding spherical harmonics coefficient to be solved. Generally, larger N (maximum of n) can induce more accurate reconstruction and finer micro-morphology. Indeed, $N = 12$ is enough to reconstruct a reliable result for many applications [33].

The spherical harmonics function $Y_n^m(\theta,\varphi)$ is given by

$$Y_n^m(\theta,\varphi) = \sqrt{\frac{2n+1(n-m)!}{4\pi(n+m)!}} P_n^m(\cos\theta) e^{im\varphi}, \tag{3}$$

where $i = \sqrt{-1}$ and $P_n^m(\cos\theta)$ is the associated Legendre function with degree n and order m, defined as

$$P_n^m(x) = (-1)^m (1-x^2)^{\frac{m}{2}} \frac{d^m}{dx^m} P_n(x), \tag{4}$$

where $P_n(x)$ is the Legendre polynomial of degree n.

As mentioned above, Polar coordinates and Cartesian coordinates are two types of representation for SH expansion. SH expansion based on Polar coordinates can only process star-shaped objects, while the second method is more versatile for not only star-shaped objects but also objects with more complex structure, e.g. concave surfaces. In this study, SH expansion based on Cartesian coordinates is used to ensure the generality of the method. For non-star-shaped particles, where the polar and azimuthal angles are not uniquely associated with the radial distance, it is necessary to perform spherical parameterization of the particle surface. This involves mapping each point on the particle surface to a corresponding point on the unit sphere surface. As shown in Fig. 2, point P on a particle surface is mapped to point Q of the unit sphere. Spherical parameterization, spherical harmonics expansion, and morphological analysis are basic procedures for particle characterization and are introduced in the following sections.

3.2. Spherical parameterization

Spherical parameterization aims to create a continuous and uniform mapping from the object surface to the surface of a unit sphere. A minimization of length distortion, angle distortion, and area distortion are required for a good mapping [34]. Numerous researchers have proposed various methods for spherical parameterization. Shen and Makedon [34] have developed a CALD (control of area and length

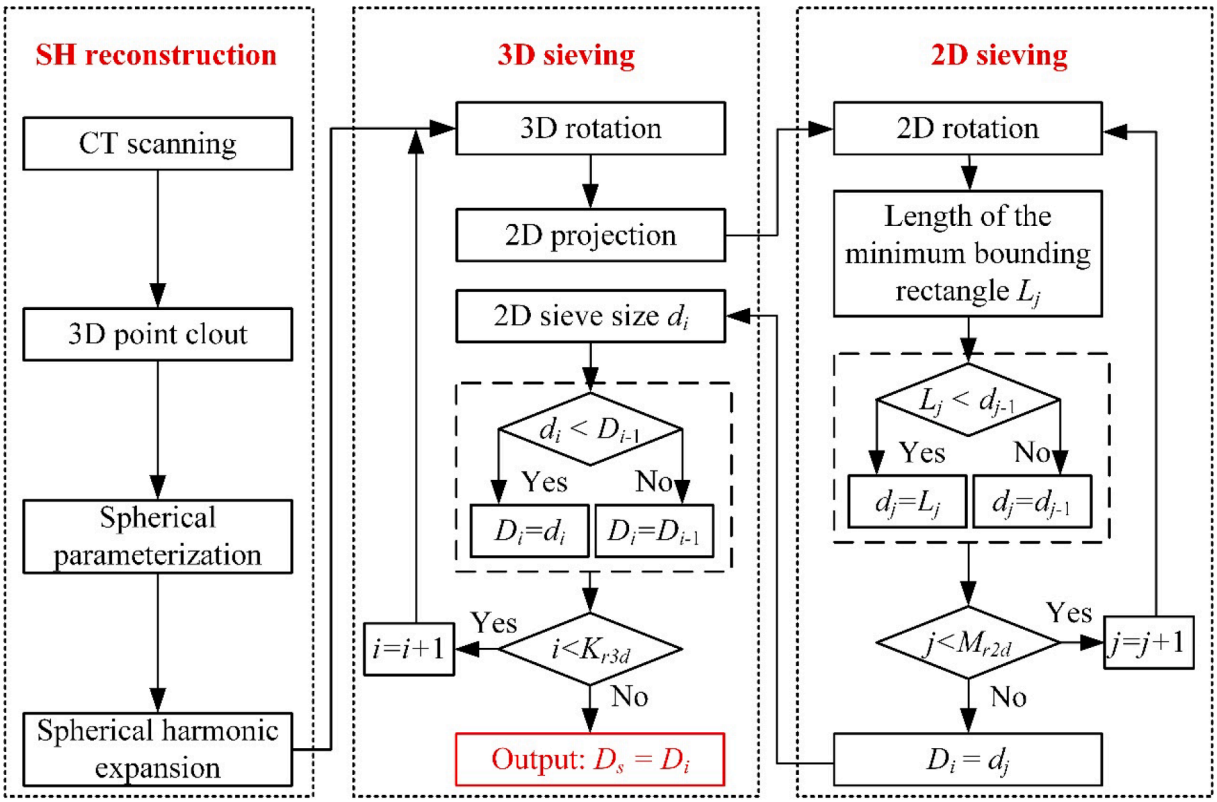

Fig. 3. Flowchart of determining particle sieve size.

distortions) algorithm, which is embedded in their SHARM-MAT, a Matlab based and widely used toolkit. Hu et al. [35] proposed a practically robust method AHSP (advanced hierarchical spherical parameterization) to compute high-quality spherical parameterization with bijection and low isometric distortion, which has been used in solid waste shape description [36]. Choi et al. [37] proposed a fast algorithm called FLASH to compute the optimized spherical harmonic parameterization with consistent landmark alignment. It should be noted that the aforementioned parameterization methods are only applicable to Genus-0 surfaces. FLASH was adopted in this study. The quality of mapping in spherical parameterization can be evaluated by the length distortion, angle distortion, and area distortion. After mapping the set of surface points **V** on particles to the unit sphere, a one-to-one correspondence is established between the coordinates of points on the particle surface and the polar angle θ and azimuthal angle φ in the spherical coordinate system.

$$v(\theta,\varphi) = (x(\theta,\varphi), y(\theta,\varphi), z(\theta,\varphi))^T. \tag{5}$$

3.3. Spherical harmonic expansion

The purpose of spherical harmonic expansion is to determine the spherical harmonic coefficients a_n^m, which encapsulate all the information about particle morphology. After parameterization, x, y and z coordinates of each point on the particle surface are expressed as an expansion of the spherical harmonic series

$$\begin{cases} x(\theta,\varphi) = \sum_{n=0}^{N}\sum_{m=-n}^{n} a_{nx}^m Y_n^m(\theta,\varphi) \\ y(\theta,\varphi) = \sum_{n=0}^{N}\sum_{m=-n}^{n} a_{ny}^m Y_n^m(\theta,\varphi) \\ z(\theta,\varphi) = \sum_{n=0}^{N}\sum_{m=-n}^{n} a_{nz}^m Y_n^m(\theta,\varphi) \end{cases}. \tag{6}$$

The above equations can be expressed in vector form as follows

$$\boldsymbol{v}(\theta,\varphi) = \sum_{n=0}^{N}\sum_{m=-n}^{n} a_n^m Y_n^m(\theta,\varphi), \tag{7}$$

where $a_n^m = \left(a_{nx}^m, a_{ny}^m, a_{nz}^m\right)^T$. Substituting all the parameterized surface point coordinates into the above equation yields the expression in matrix form [38]

$$\begin{pmatrix} x_1 & y_1 & z_1 \\ x_2 & y_2 & z_2 \\ \vdots & \vdots & \vdots \\ x_K & y_K & z_K \end{pmatrix} = \begin{pmatrix} Y_1^1 & Y_1^2 & \cdots & Y_1^{(N+1)^2} \\ Y_2^1 & Y_2^2 & \cdots & Y_2^{(N+1)^2} \\ \vdots & \vdots & \vdots & \vdots \\ Y_K^1 & Y_K^2 & \cdots & Y_K^{(N+1)^2} \end{pmatrix} \begin{pmatrix} a_x^1 & a_y^1 & a_z^1 \\ a_x^2 & a_y^2 & a_z^2 \\ \vdots & \vdots & \vdots \\ a_x^{(N+1)^2} & a_y^{(N+1)^2} & a_z^{(N+1)^2} \end{pmatrix}, \tag{8}$$

where K is the total number of the points. When the highest degree is N, the total number of each component of SH coefficient a_n^m is $(N+1)^2$. $\left[Y_i^1, Y_i^2, \ldots, Y_i^{(N+1)^2}\right]$ is a one dimensional array, reshaped by $\left[Y_n^m(\theta_i,\varphi_i)\right]$. Moreover, Eq. (8) can be written as the following linear relation

$$\mathbf{YA} = \mathbf{V}. \tag{9}$$

Matrix **A** can be solved by singular value decomposition (SVD) as

$$\mathbf{A} = \left(\mathbf{Y}^T\mathbf{Y}\right)^{-1}\mathbf{Y}^T\mathbf{V}. \tag{10}$$

Alternatively, the solution can also be obtained directly by matrix left division

$$\mathbf{A} = \mathbf{Y}/\mathbf{V}. \tag{11}$$

Both of the two methods can be easily implemented in Matlab. Note that for the computation of spherical harmonic coefficients in terms of radial distance, Gaussian quadrature methods can also be employed in addition to the methods mentioned above [33]. Eq. (8) has only solution when $K \geq (N+1)^2$. In general, the number of parameterized surface

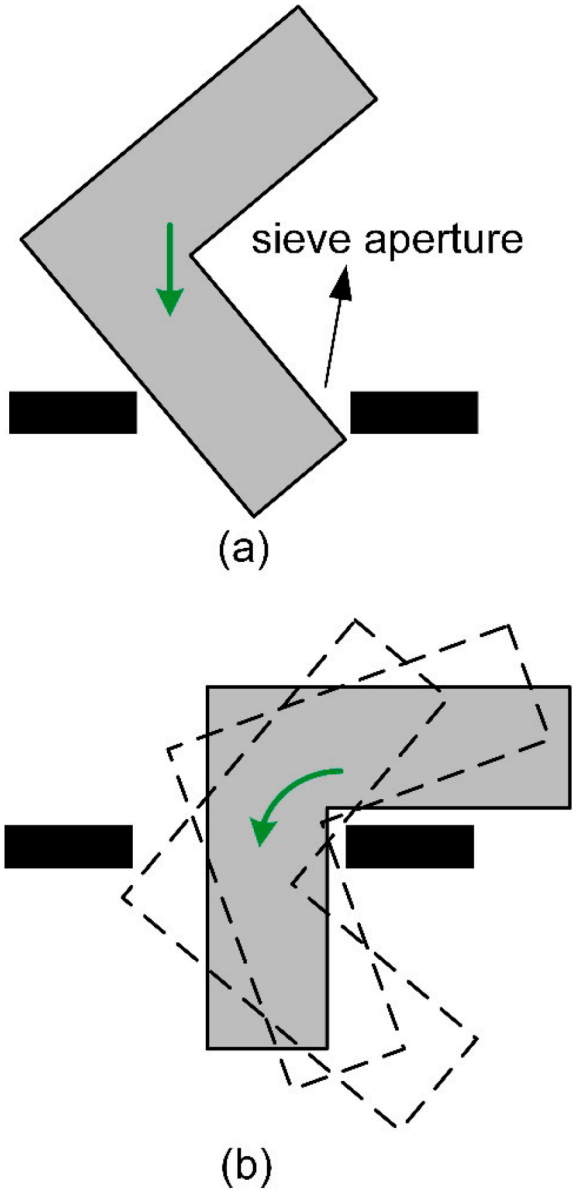

Fig. 4. (a) L-shaped particle in a particular orientation cannot pass through the sieve aperture. (b) Particle in a certain orientation can partially pass through the sieve aperture. Simultaneously, by adjusting their orientation through rotation, they can transition through the sieve aperture.

points is often sufficiently large to satisfy the solving requirements. Thus, the upper limit of N is $\left[\sqrt{K}-1\right]$ where represents the round down symbol.

3.4. Morphological analysis

Upon acquisition of spherical harmonic coefficients, the reconstruction and analysis of three-dimensional morphological properties of coal powder become achievable. The vector representing the reconstructed surface point to the particle centroid can be expressed as

$$\overrightarrow{S} = v(\theta,\varphi)^T - v_0(\theta,\varphi)^T, \tag{12}$$

where $v_0(\theta,\varphi)^T$ is the particle centroid, obtained from the 0 degree ($N=0$) expansion. Drawing upon classical differential geometry principles, one can employ partial derivatives of surface functions to compute morphological parameters [39]. The surface normal vector is expressed as

$$\widehat{n} = \frac{\overrightarrow{S_\theta} \times \overrightarrow{S_\varphi}}{\left|\overrightarrow{S_\theta} \times \overrightarrow{S_\varphi}\right|}, \tag{13}$$

where $\overrightarrow{S_\theta}$ and $\overrightarrow{S_\varphi}$ are the partial derivatives of $\overrightarrow{S}$ with respect to θ and φ

$$\overrightarrow{S}_\theta = \sum_{n=0}^{N}\sum_{m=-n}^{n} a_n^m \frac{\partial Y_n^m(\theta,\varphi)}{\partial\theta}, \tag{14}$$

$$\overrightarrow{S}_\varphi = \sum_{n=0}^{N}\sum_{m=-n}^{n} a_n^m \frac{\partial Y_n^m(\theta,\varphi)}{\partial\varphi}. \tag{15}$$

The second partial derivatives of $\overrightarrow{S}$ are similar. Both of the first and second partial derivatives can be computed using the recursion method [40].

The total particle surface area is given by

$$A = \int_0^{2\pi}\int_0^{\pi} \left|\overrightarrow{S_\theta} \times \overrightarrow{S_\varphi}\right| \mathrm{d}\theta\mathrm{d}\varphi. \tag{16}$$

The total particle volume is given by

$$V = \frac{1}{3}\int_0^{2\pi}\int_0^{\pi} \left(\overrightarrow{S}\cdot\widehat{n}\right)\left|\overrightarrow{S_\theta} \times \overrightarrow{S_\varphi}\right| \mathrm{d}\theta\mathrm{d}\varphi. \tag{17}$$

The diameter of volume equivalent sphere D_{ves} is calculated as

$$D_{ves} = \sqrt[3]{\frac{6V}{\pi}}. \tag{18}$$

Furthermore, the sphericity index (SI) of the particle can be calculated from the volume and surface area results as

$$\mathrm{SI} = \frac{\sqrt[3]{36\pi V^2}}{A}. \tag{19}$$

The specific surface area (SSA) is also a important parameter for fuel particle, defined as the ratio of particle surface area and volume

$$\mathrm{SSA} = \frac{A}{V}. \tag{20}$$

Three principal dimensions, that is, the long axis L, the intermediate axis W, and the short axis T, are significant to evaluate irregular particle form. Through principal component analysis (PCA), once the three principal directions of the particle are determined, the particle can be rotated such that each principal axis aligns with one of the Cartesian coordinate axes. The difference between the maximum and minimum coordinate values along each direction represents the main scale for that direction. Ordering these three main scales from largest to smallest results in the major axis, intermediate axis, and minor axis of the particle [41]. The enlongation index (EI) and flatness index (FI) are two aspect ratios proposed by Zingg [42] to describe and classify irregular particle shape. The enlongation index and flatness index are defined as

$$\mathrm{EI} = W/L, \tag{21}$$

$$\mathrm{FI} = T/W, \tag{22}$$

The two indexes range from 0 to 1. The particle become more compact when EI and FI approach 1.

Mechanical sieving, as a simple and low-cost method for particle size analysis, has been used widely in laboratory and industrial process. The sieve size is also a noteworthy parameter in particle characterization. However, it is difficult to determine using other methods except the physical sieving process. Rotation invariant spherical harmonic representation provides an effective solution. This approach enables the analysis of irregular particle sizes for each reconstructed particle, facilitating the examination of correlations between sieve sizes and various size or shape parameters.

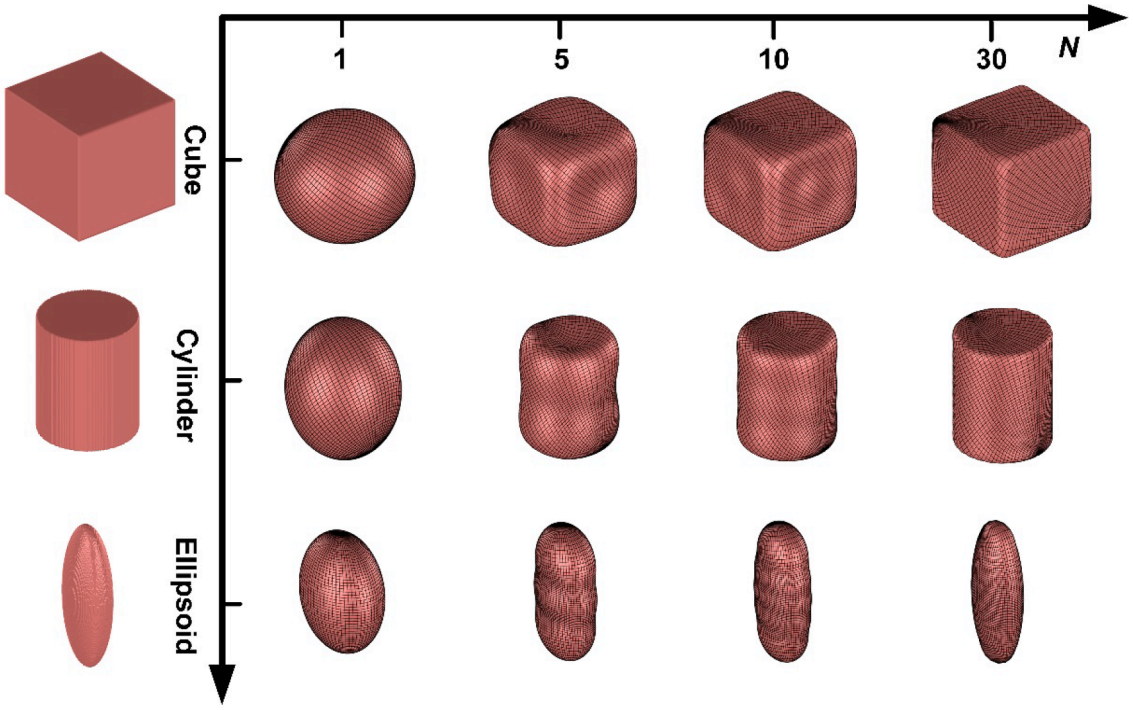

Fig. 5. Reconstructed shape of cube, cylinder, and ellipsoid under various degrees *N*.

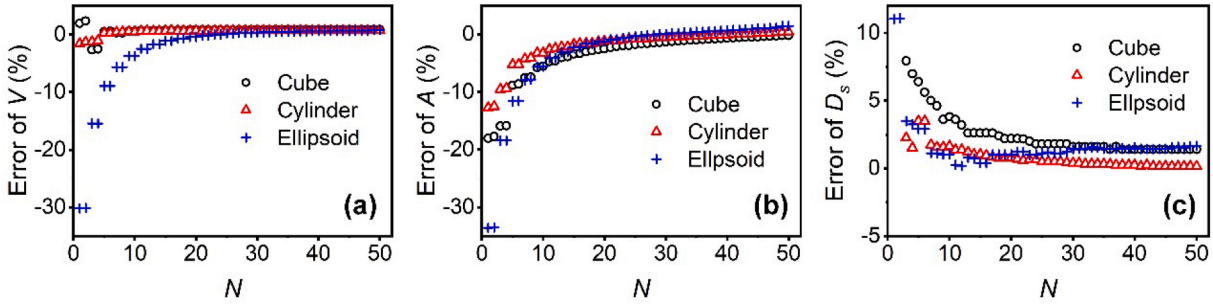

Fig. 6. (a) Volume, (b) surface area, and (c) sieve size error of the three reconstructed standard geometries.

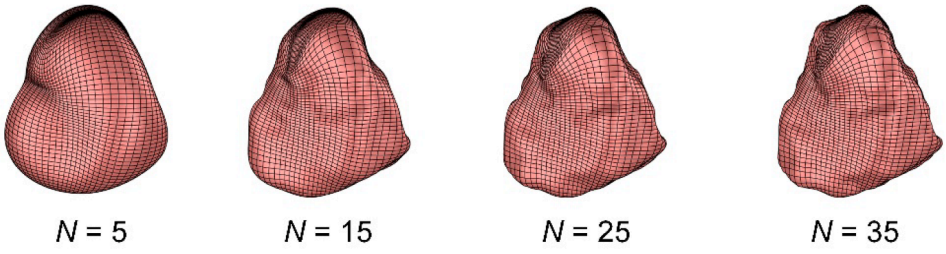

Fig. 7. Reconstructed shapes of a coal particle under various degrees *N*.

This paper has proposed a algorithm to determine particle sieve size based on SH reconstruction. The algorithm flowchart is shown in Fig. 3. In real sieving process, an irregular particle passes through the sieve mesh by precision, rotation, and translation [21]. The sieve size D_s is defined as the edge length of the smallest quadratic aperture, through which the particle can pass in one direction at least [43]. Throughout this process, particles exhibit a series of orientations, each of which corresponds to a sieve aperture size that allows the particle to pass through. The smallest sieve aperture size among these orientations is the particle sieve size, which represents the effective size during sieving. This algorithm is based on simulating this physical process to determine the sieve size. However, it is important to note that this method simplifies complex sieving processes. It assumes that particles can only pass through the sieve aperture by translating downward in a specific orientation, without simultaneous translational and rotational adjustments. This is because the dynamic process involving both translation and rotation is intricate and challenging to accurately describe. This assumption can be illustrated by considering the L-shaped particle passing through the sieve aperture in Fig. 4. In Fig. 4 (a), the L-shaped particle can only pass through the sieve aperture in a specific orientation. Due to its overall size being larger than the sieve opening, it cannot pass through regardless of its orientation. However, if it dynamically

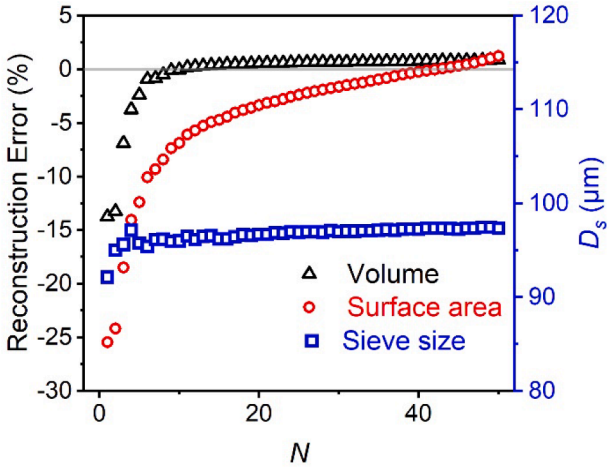

Fig. 8. Volume, surface area and sieve size errors of a coal powder.

adjusts its orientation as shown in Fig. 4 (b), with a portion of the particle passing through the sieve aperture while undergoing a rotational adjustment, it can eventually pass through. Nevertheless, this process is highly dependent on the specific morphology of the particle and involves a complex model that is difficult to implement. Furthermore, most industrial powders are not of this bent bar-like structure but are predominantly close to spherical or convex particles. Simplifications of the sieving process can be applied for most cases except for certain biomass or fiber particles.

The core idea of this algorithm involves rotating the particle at different angles (around the *x*,*y*, and *z* axis). The particle morphology at each angle corresponds to a particle sieve size, with the minimum value being the 3D sieve size. The sieve size at each angle corresponds to the minimum bounding square of the two-dimensional projection, which can be obtained through the minimum bounding rectangle (MBR). Due to the rotational invariance of SH, rotating a particle in 3D involves multiplying its SH coefficients by a rotation matrix, eliminating the need to transform the coordinates of the 3D point cloud. The rotation matrices for rotation around the *x*,*y*, and *z* axis are as follows

$$R_x = \begin{pmatrix} 1 & 0 & 0 \\ 0 & \cos\alpha & -\sin\alpha \\ 0 & \sin\alpha & \cos\alpha \end{pmatrix}$$
$$R_y = \begin{pmatrix} \cos\beta & 0 & \sin\beta \\ 0 & 1 & 0 \\ -\sin\beta & 0 & \cos\beta \end{pmatrix}. \quad (23)$$
$$R_z = \begin{pmatrix} \cos\gamma & -\sin\gamma & 0 \\ \sin\gamma & \cos\gamma & 0 \\ 0 & 0 & 1 \end{pmatrix}$$

The overall rotation matrix is the product of these three individual rotation matrices

$$R = R_x \cdot R_y \cdot R_z. \quad (24)$$

The spherical harmonics coefficients b_n^m after rotation is expressed as

$$b_n^m = a_n^m \cdot R. \quad (25)$$

Rotated particle can be reconstructed using b_n^m. Considering the symmetry, setting rotation angles in the range of 0 to 90 degrees is sufficient. For instance, if an angle is taken every 3 degrees, there would be 30 angles for each coordinate axis. This results in a total of $30 \times 30 \times 30 = 27{,}000$ angle combinations, requiring 27,000 rotations in total. Indeed, through comparison, we found that the angle interval has a minor impact on the sieve size results (within 1 %). To improve computational speed, larger angle intervals can be employed. We denote the total number of rotations as K_{r3d}. Smaller angle intervals yield more accurate results, but computation time will significantly increase.

Then the rotated particle is projected to *x*-*y* plane and the sieve size of the 2D projection is obtained. Using the *boundary* function in MATLAB, one can obtain a two-dimensional projection of 3D data. However, the obtained data might not be in integer points, so an interpolation method is used to convert the 2D projection into an image, enabling subsequent image processing operations. The sieve size of the 2D projection is determined by the minimum bounding rectangle obtained through rotation, where rotations are performed by rotating the projection around its geometric center in a clockwise manner. The rotation angle range is also 0 to 90 degrees, and the total number of rotations is

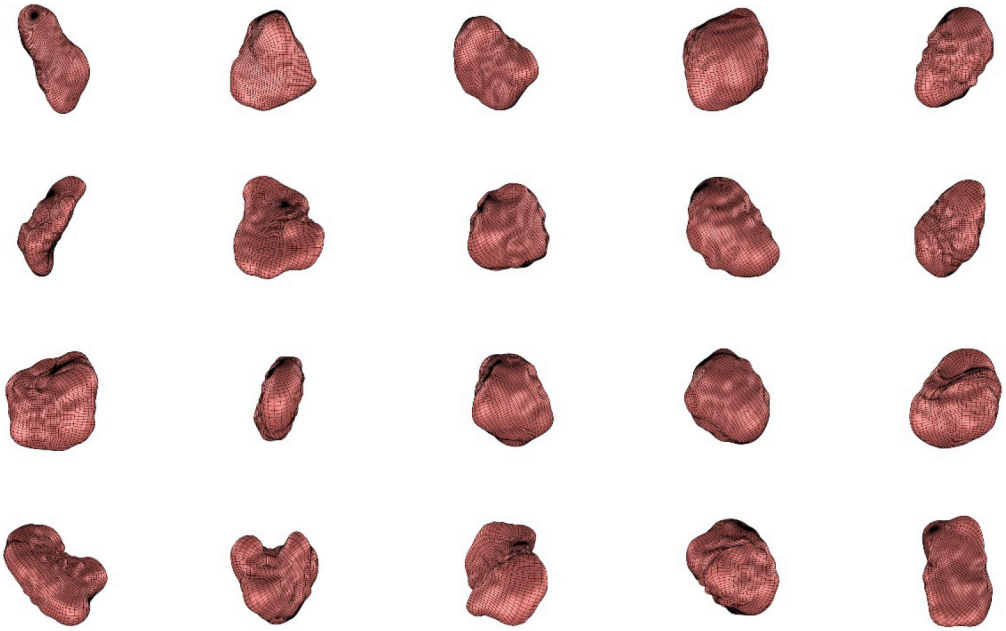

Fig. 9. Several reconstructed coal particles.

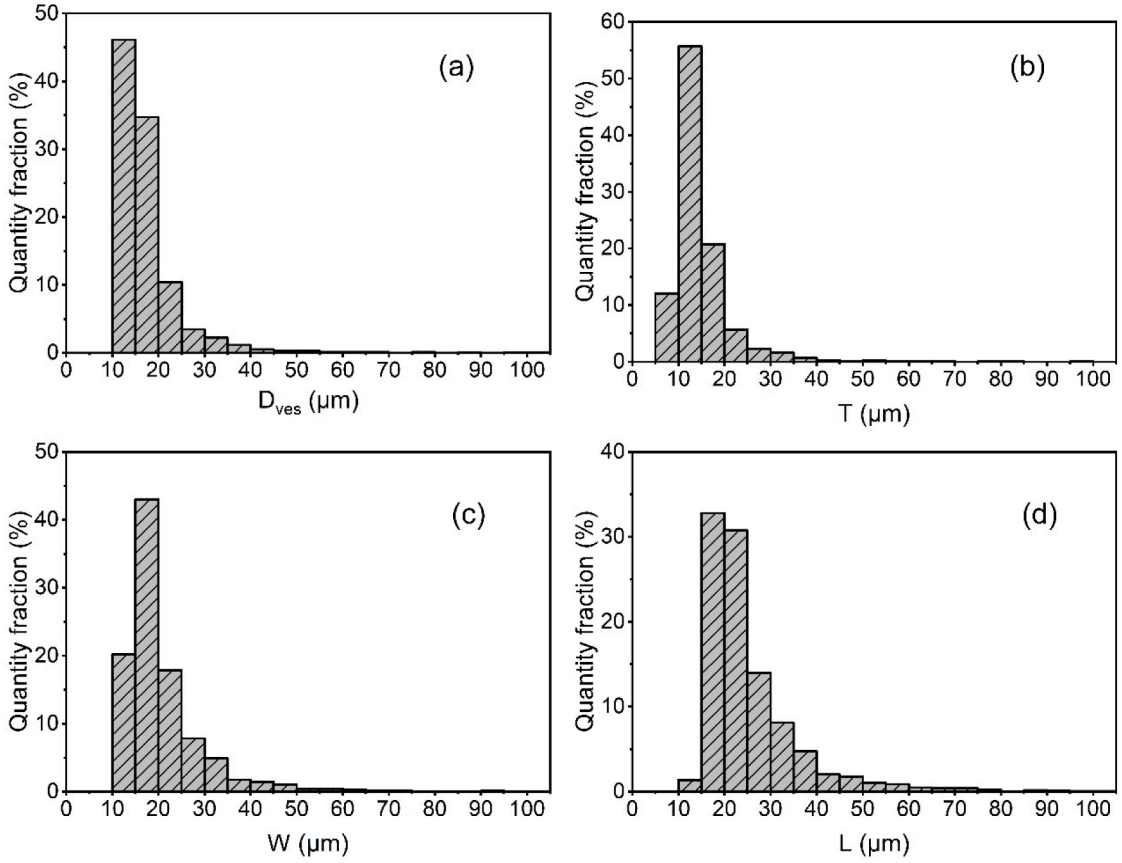

Fig. 10. Quantity distributions of (a) D_{ves}, (b) T, (c) W, and (d) L.

denoted as M_{r2d}. After each rotation, the length L_j of the bounding rectangle is obtained, and the minimum of L_j across all rotations represents the sieve size d_i of the 2D projection. The smallest d_i among all 2D projections can be considered the 3D sieve size D_s.

3.5. Method validation

Three standard geometries including a cube, cylinder, and ellipsoid were generated numerically to validate the accuracy of SH method for particle characterization. By comparing the theoretical volume and surface area to the reconstructed values with SH, one can assess the errors under various spherical harmonic degrees N. The side length of the cube was 50. The bottom radius and height of the cylinder were 40 and 100. Three half axis lengths of the ellipsoid were 100, 40, and 25, respectively. Volumes and surface areas of the geometries can be calculated by theoretical formula or approximate formula (for ellipsoid).

Fig. 5 depicts reconstructed morphology of the cube, cylinder, and ellipsoid under various degrees N. It is obvious that, as N increases, the reconstructed shape becomes increasingly similar to the true shape. When N reaches 30, the reconstructed shape closely aligns with the true shape, achieving a nearly identical match. Reconstructed volume and surface area at different SH degrees N were calculated according to Eq. (16) and Eq. (17), and the relative errors were evaluated, as shown in Fig. 6(a) and (b). As N increases, the reconstruction volume error converges rapidly, especially for cube and cylinder shapes. At around $N = 10$, the volume reconstruction error is already below 0.6 %, while for ellipsoid shapes, achieving a similar accuracy requires an N of around 20 or more. Surface area reconstruction error is significantly larger compared to volume and converges more slowly. The convergence trend for all three geometric shapes is similar. At around $N = 20$, the surface area reconstruction error for all three shapes is less than 3 %. It is worth noting that for cylinder and ellipsoid shapes, the surface area reconstruction error does not fully converge to 0 when N is greater than 30. Instead, it slightly increases. However, until $N = 50$, the error remains within $\pm$ 2 %. The errors of sieve size are shown in Fig. 6(c) which are less than 2.5 % when $N \geq 20$. Considering the accuracy of both volume and surface area along with computational speed, this study selects an N value of 20 for the highest degree of spherical harmonic reconstruction.

4. Results and discussions

Fig. 7 shows the reconstructed shapes of a typical coal particle under different degrees N. It is clear that the microscopic surface morphology of particles is more comprehensively represented, as the degree of spherical harmonics increases. For comparison, image-based particle volume and surface area were also obtained using *bwconncomp* and *regionprops3* functions. The relative errors between the SH-based and image-based results are plotted in Fig. 8. Similar to the results for regular geometric shapes, the volume reconstruction accuracy is higher than the surface area accuracy. With a reconstruction degree of $N = 20$, the relative errors for volume and surface area are 0.85 % and −3.36 %, respectively. The change in the sieve size across different SH degrees is minimal, almost within 1 %.

Furthermore, 1709 valid coal particles were reconstructed and analyzed. Fig. 9 displays the reconstructed shapes of some coal powder particles. The morphology of coal powder particles varies widely, ranging from nearly spherical to rod-like or flattened shapes. Some coal powder particles exhibit intricate surface features, including several concavities. It is evident that coal powder particles possess complex and diverse morphologies, characterized by extreme irregularity. This complexity presents challenges in accurately and effectively measuring their particle size.

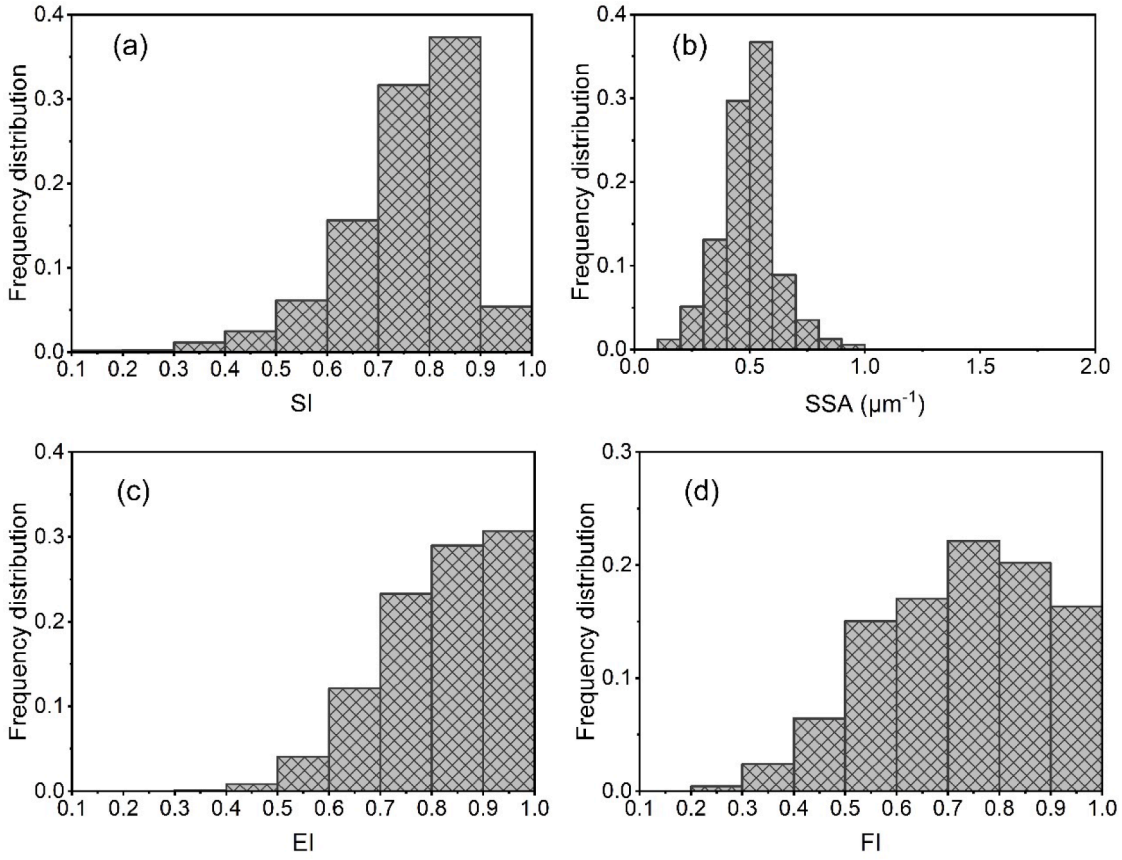

Fig. 11. Quantity distributions of (a) SI, (b) SSA, (c) EI, and (d) FI.

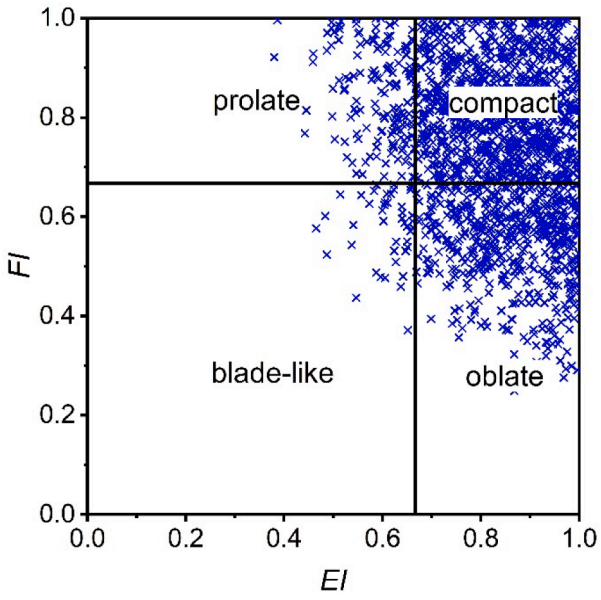

Fig. 12. Shape classification of measured coal powder in Zingg diagram.

4.1. Size analysis

Fig. 10 shows the quantity distributions of D_{ves}, T, W, and L. Coal particles with diameter ranging from 10 μm to 20 μm occupied over 80 %. Particle size distribution results of the coal powder sample obtained using the developed digital holographic particle analyzer (DHPA) [44] indicated that the proportion in the range of 10–20 μm is also the highest, reaching 43 %.

The peak sizes of T, W, and L were about 10–15 μm, 15–20 μm, and 15–25 μm, respectively. Furthermore, relative relation of the diameter of volume equivalent sphere and the three principal dimensions was analyzed. It was found that the average values of size ratios D_{ves}/T, D_{ves}/W, and D_{ves}/L were 1.23, 0.86, and 0.70, indicating that D_{ves} was closer to the intermediate axis.

4.2. Shape analysis

Fig. 11 shows the quantity distributions of SI, SSA, EI, and FI. The results indicate that most coal powder particles have SI ranging from 0.7 to 0.9, SSA predominantly falling in the range of 0.4 μm^{-1} to 0.6 μm^{-1}, EI generally exceeding 0.7, and FI distributed fairly evenly in the range of 0.5 to 1.0. The average SI is 0.76 which is consistent with the approximate range of coal particle sphericity reported in the literature [45], although the literature typically employs two-dimensional measurement methods. The average SSA is 0.51 μm^{-1}. If the particles were all spherical, the average SSA would be 0.37 μm^{-1} theoretically. The average EI is 0.82, and the average FI is 0.73. Based on the EI and FI, particle shapes can be classified using a Zingg diagram, as shown in Fig. 12. It is demonstrated that most coal powder particles are either nearly spherical (more than 60 %) or oblated. This suggests that ellipsoids or flat spheroids could be employed for modeling coal powder particles in studies related to combustion and similar research areas.

4.3. 3D sieving

The reconstructed coal particles were sieved digitally with the proposed method to determine the 3D sieve size based on spherical harmonics. Fig. 13 depicts detailed procedures of 3D digital sieving. Firstly, 3D particle shape was reconstructed by SH as shown in Fig. 13(a). The

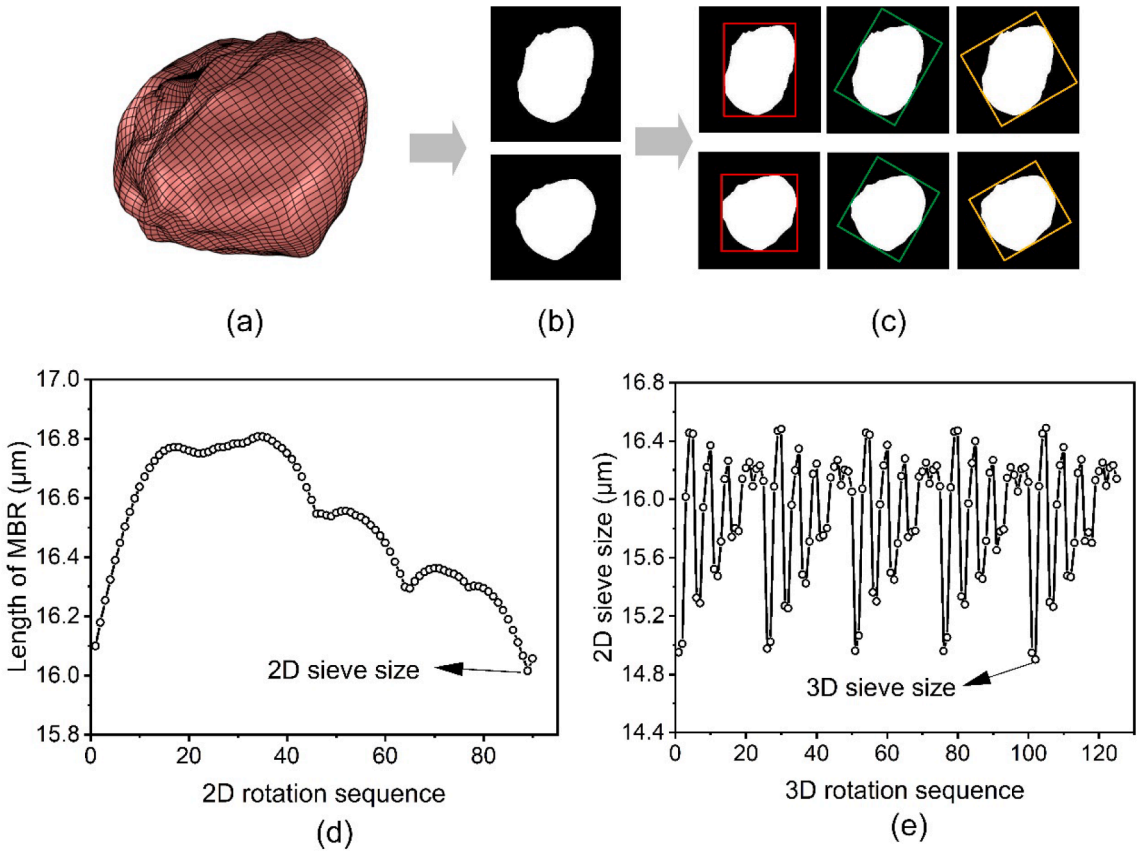

Fig. 13. Determination of 3D sieve size based on spherical harmonics. (a) A reconstructed coal particle. (b) 2D projections after rotations. (c) Determination of 2D sieve size by rotating the projections and searching the minimum bounding rectangle. (d) Lengths of the minimum bounding rectangles in the 2D rotation sequence. (e) 2D sieve size in the 3D rotation sequence.

images in Fig. 13(b) are the 2D projections of the rotated particle. Fig. 13 (c) depicts how a 2D sieve size of a projection is determined by searching the minimum length of the bounding squares (Fig. 13(d)). Ultimately, the minimum of the 2D sieve sizes was regarded as the 3D sieve size (Fig. 13(e)).

The quantity distribution of the 3D sieve size D_s (Fig. 14) was closely aligned with the distribution of D_{ves} in Fig. 10(a). In order to investigate the relationships between D_s and D_{ves} of particles with different shapes, we took the ratio D_s/D_{ves} as an indicator. Fig. 14(b), (c), and (d) illustrate the influences of SI, EI, and FI$ on D_s/D_{ves}, respectively. The results reveal that there appears to be a stronger correlation between SI and EI with D_s/D_{ves}. Fig. 14(b) shows that D_s/D_{ves} concentrates between 0.8 and 1.2 when SI $>$ 0.5.

4.4. Comparison of 3D and 2D measurements

The current commonly used particle analysis techniques can be classified into two categories. The first category, based on the assumption of spherical particle, including such as laser diffraction, sedimentation, and sieving, cannot measure particle shape directly, and the results are influenced by shape. The second category, such as dynamic image analysis, scanning electron microscopy, and holographic imaging, directly captures actual particle images but is limited to 2D projection images. For spherical particles, 2D projections can reflect the true particle size. However, for non-spherical particles, results based on 2D projection images may vary with different projection angles. These methods yield different particle size and shape results due to differences in technical principles. Thus, particle characterization may be ambiguous without a comparison with the actual particle size distribution and morphology obtained from standard techniques.

It is assumed that 2D projection images recorded at different angle of view are equally probable, when using 2D imaging methods such as digital holography (DH) and digital imaging analysis (DIA). Hence we can use the average projections of a rotated particle at various angles introduced in Section 3.4 to represent the expected 2D measurement. The diameter of area equivalent circle D_{aec} represents the measured particle size by 2D imaging methods. We analyzed the correlations between D_s and D_{aec} and D_{ves}. Linear regressions were performed on the scatter plots of D_s versus D_{ves} and D_s versus D_{aec} in Fig. 15, and linear correlations can be clearly observed. Taken as a whole, the equivalent volume sphere particle size appears to be smaller than the sieve size, while the equivalent projection area circle diameter appears to be larger than the sieve particle size. The volume-based size distributions of D_s, D_{ves} and D_{aec} are plotted in Fig. 16. The statistical analysis demonstrated that, volume fraction of large particles will be overestimated with D_{aec}. In terms of coal fineness, which is defined by the sieving method and denoted by R_{90} (mass proportion of particles larger than 90 μm) in coal-fired power plant, fineness result based on D_s, D_{ves} and D_{aec} were 10.25 %, 11.47 %, and 13.93 %, respectively.

5. Conclusions

Accurate morphology characterization of fuel particles plays a significant role in fuel processing, conversion, and combustion studies. Particle shape, particularly in three dimensions, can serve as valuable guidance for the measurement of particle size distribution. In this work, 3D morphology of micron-sized pulverized coal, a typical solid fuel, was characterized with XRCT and SH. The main conclusions are summarized as follows.

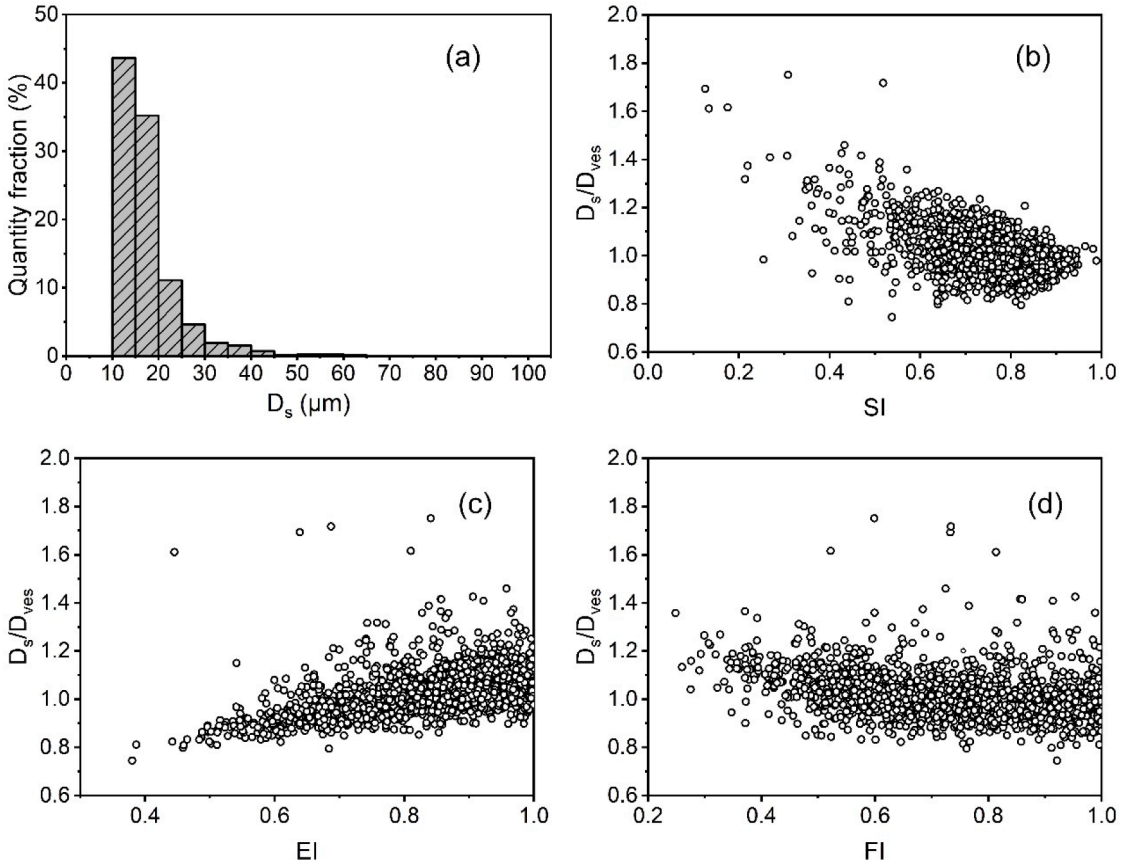

Fig. 14. (a) Quantity distribution of D_s. Relationships between D_s / D_{ves} and (b) SI, (c) EI, and (d) FI.

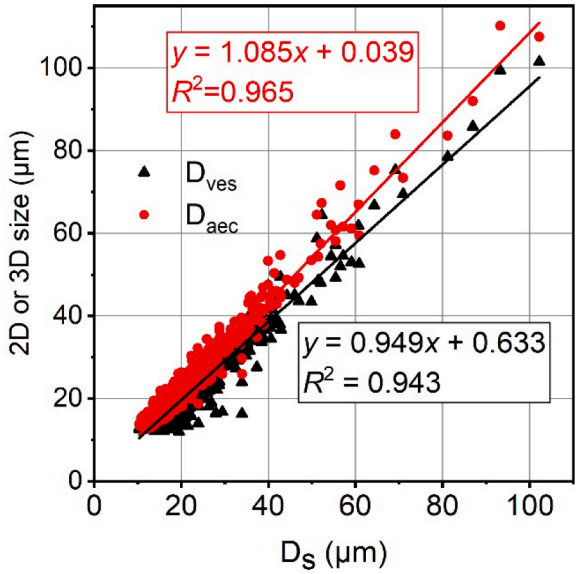

Fig. 15. The relationship between 3D sieve size D_s and D_{ves} and D_{aec}.

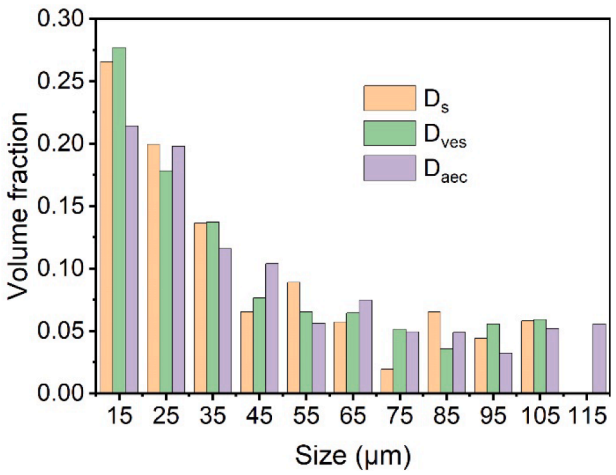

Fig. 16. Comparison of volume based particle size distribution of D_s, D_{ves}, and D_{aec}.

- The fundamental principles and algorithms of particle 3D morphology characterization based on XRCT and SH were outlined. An algorithm based on the rotation invariance of SH for determining the actual sieve size of irregular particles was proposed. The accuracy of the method was validated using standard geometries. The volume errors, surface area errors, and sieve size errors were within 1 %, 3 %, and 2.5 %, respectively, when the SH degree $N \geq 20$.
- A micron-sized coal powder sample was characterized with XRCT and SH. With a reconstruction degree of $N = 20$, the relative errors for volume and surface area were 0.85 % and −3.36 %, respectively, which verified the reliability of the method for reconstructing coal powder. Most of the particles exhibited sphericities within the range of 0.7 to 0.9, and the specific surface area primarily fell within the range of 0.4 μm^{-1} to 0.6 μm^{-1}. The Zingg diagram for particle shape classification indicated that the majority of coal powder particles were either nearly spherical or oblated.

- When comparing the average result of 2D particle size using equi-probable projections with the actual 3D particle size, it was observed that, overall, D_{ves} was smaller than D_s, while the D_{aec} was larger than D_s. The coal powder fineness measured based on D_{aec} was the highest. The D_{aec} of 2D projection was approximately 1.12 times more than D_{ves}. The results indicated that coal powder fineness measurement based on 2D projections may overestimate the fineness.

CRediT authorship contribution statement

Qiwen Jin: Writing – original draft, Software, Investigation, Formal analysis, Data curation. **Zhiming Lin:** Writing – review & editing, Formal analysis. **Yingchun Wu:** Writing – review & editing, Conceptualization. **Xuecheng Wu:** Writing – review & editing, Supervision, Resources, Funding acquisition, Conceptualization.

Declaration of competing interest

The authors declare that they have no known competing financial interests or personal relationships that could have appeared to influence the work reported in this paper.

Data availability

Data will be made available on request.

Acknowledgement

The authors gratefully acknowledge the support from the Fundamental Research Funds for the Central Universities (No.2022ZFJH04), the Innovative Research Groups of the National Natural Science Foundation of China (No.51621005), the Program of Introducing Talents of Discipline to University (No.BP0820002).

References

[1] Liu J, Jiang X, Huang X, Wu S. Morphological characterization of superfine pulverized coal particles. 1. Fractal characteristics and economic fineness. Energy Fuel 2010;24(2):844–55.
[2] Wang Q, Wang E. Numerical investigation of the influence of particle shape, pretreatment temperature, and coal blending on biochar combustion in a blast furnace. Fuel 2022;313:123016.
[3] Tabet F, Gkalp I. Review on CFD based models for co-firing coal and biomass. Renew Sustain Energy Rev 2015;51:1101–14.
[4] Bonefacic I, Frankovic B, Kazagic A. Cylindrical particle modelling in pulverized coal and biomass co-firing process. Appl Therm Eng 2015;78:74–81.
[5] Schiemann M, Haarmann S, Vorobiev N. Char burning kinetics from imaging pyrometry: particle shape effects. Fuel 2014;134:53–62.
[6] Pragadeesh KS, Regupathi I, Sudhakar DR. Study of devolatilization during chemical looping combustion of large coal and biomass particles. J Energy Inst 2020;93(4):1460–72.
[7] Momeni M, Yin C, Kr SK, Hansen TB, Jensen PA, Glarborg P. Experimental study on effects of particle shape and operating conditions on combustion characteristics of single biomass particles. Energy Fuel 2013;27(1):507–14.
[8] Lu H, Ip E, Scott J, Foster P, Vickers M, Baxter LL. Effects of particle shape and size on devolatilization of biomass particle. Fuel 2010;89(5):1156–68.
[9] Ning D, Hazenberg T, Shoshin Y, van Oijen JA, Finotello G, de Goey LPH. Experimental and theoretical study of single iron particle combustion under low-oxygen dilution conditions. Fuel 2024;357:129718.
[10] Backreedy RI, Fletcher LM, Jones JM, Ma L, Pourkashanian M, Williams A. Co-firing pulverised coal and biomass: a modeling approach. Proc Combust Inst 2005;30(2):2955–64.
[11] Zhang W, Watanabe H, Kitagawa T. Numerical investigation of effects of particle shape on dispersion in an isotropic turbulent flow. Adv Powder Technol 2018;29(9):2048–60.
[12] Zhou J-w, Liu Y. Du C-l, Liu S-y. Effect of the particle shape and swirling intensity on the breakage of lump coal particle in pneumatic conveying. Powder Technol 2017;317:438–48.
[13] Grubbs J, Tsaknopoulos K, Massar C, Young B, O'Connell A, Walde C, et al. Comparison of laser diffraction and image analysis techniques for particle size-shape characterization in additive manufacturing applications. Powder Technol 2021;391:20–33.
[14] Silva AFT, Burggraeve A, Denon Q, Van der Meeren P, Sandler N, Van Den Kerkhof T, et al. Particle sizing measurements in pharmaceutical applications: Comparison of in-process methods versus off-line methods. Eur J Pharm Biopharm 2013;85(3):1006–18.
[15] Gil M, Teruel E, Arauzo I. Analysis of standard sieving method for milled biomass through image processing. Effects of particle shape and size for poplar and corn stover. Fuel 2014;116:328–40.
[16] Trubetskaya A, Beckmann G, Wadenbck J, Holm JK, Velaga SP, Weber R. One way of representing the size and shape of biomass particles in combustion modeling. Fuel 2017;206:675–83.
[17] Ulusoy U, Igathinathane C. Dynamic image based shape analysis of hard and lignite coal particles ground by laboratory ball and gyro mills. Fuel Process Technol 2014;126:350–8.
[18] Igathinathane C, Ulusoy U. Machine vision methods based particle size distribution of ball-and gyro-milled lignite and hard coal. Powder Technol 2016;297:71–80.
[19] Ulusoy U, Igathinathane C. Particle size distribution modeling of milled coals by dynamic image analysis and mechanical sieving. Fuel Process Technol 2016;143:100–9.
[20] Yang X, Ren T, Tan L. Size distribution measurement of coal fragments using digital imaging processing. Measurement 2020;160:107867.
[21] Jin Q, Chen X, Li P, Zhou Y, Wu Y, Wu X. On-line measurement of pulverized coal fineness on a 300 MWe power plant with pulsed digital inline holography. Powder Technol 2021;385:242–9.
[22] Botlhoko S, Campbell QP, le Roux M, Nakhaei F. Washability analysis of coal using RhoVol: a novel 3D image-based method. Miner Process Extr Metall Rev 2023;44(2):125–37.
[23] Yang D, Tang J, Hu N, Xia Y, Yu Y, Huang Q. The shape parameters of coal and gangue particles derived from 3D scanning. Sci Data 2023;10(1):107.
[24] Withers PJ, Bouman C, Carmignato S, Cnudde V, Grimaldi D, Hagen CK, et al. X-ray computed tomography. Nature Reviews Methods Primers 2021;1(1):18.
[25] Fonseca J, O'Sullivan C, Coop MR, Lee PD. Non-invasive characterization of particle morphology of natural sands. Soils Found 2012;52(4):712–22.
[26] Alam MF, Haque A, Ranjith PG. A study of the particle-level fabric and morphology of granular soils under one-dimensional compression using insitu X-ray CT imaging. Materials 2018;11(6):919.
[27] Zhou B, Ku Q, Wang H, Wang J. Particle classification and intra-particle pore structure of carbonate sands. Eng Geol 2020;279:105889.
[28] Garboczi EJ, Bullard JW. Shape analysis of a reference cement. Cem Concr Res 2004;34(10):1933–7.
[29] Garboczi EJ, Riding KA, Mirzahosseini M. Particle shape effects on particle size measurement for crushed waste glass. Adv Powder Technol 2017;28(2):648–57.
[30] Zhou X, Dai N, Cheng X, Thompson A, Leach R. Three-dimensional characterization of powder particles using X-ray computed tomography. Addit Manuf 2021;40:101913.
[31] Su D, Yan WM. 3D characterization of general-shape sand particles using microfocus X-ray computed tomography and spherical harmonic functions, and particle regeneration using multivariate random vector. Powder Technol 2018;323:8–23.
[32] Ji S, Liu L. Computational granular mechanics and its engineering applications. Springer; 2020.
[33] Garboczi EJ. Three-dimensional mathematical analysis of particle shape using X-ray tomography and spherical harmonics: Application to aggregates used in concrete. Cem Concr Res 2002;32(10):1621–38.
[34] Shen L, Makedon F. Spherical mapping for processing of 3D closed surfaces. Image Vis Comput 2006;24(7):743–61.
[35] Hu X, Fu X-M, Liu L. Advanced hierarchical spherical parameterizations. IEEE Trans Vis Comput Graph 2017;24(6):1930–41.
[36] Li Y, Qin X, Zhang Z, Dong H. Solid waste shape description and generation based on spherical harmonics and probability density function. Waste Manag Res 2022;40(1):66–78.
[37] Choi PT, Lam KC, Lui LM. FLASH: Fast landmark aligned spherical harmonic parameterization for genus-0 closed brain surfaces. SIAM J Imag Sci 2015;8(1):67–94.
[38] Zhou B, Wang J, Zhao B. Micromorphology characterization and reconstruction of sand particles using micro X-ray tomography and spherical harmonics. Eng Geol 2015;184:126–37.
[39] Duncan BS, Olson AJ. Approximation and characterization of molecular surfaces. Biopolymers: Original Research on Biomolecules 1993;33(2):219–29.
[40] Bosch W. On the computation of derivatives of Legendre functions. Phys Chem Earth Part A 2000;25(9–11):655–9.
[41] Zhao B, Wang J. 3D quantitative shape analysis on form, roundness, and compactness with $$CT. Powder Technol 2016;291:262–75.
[42] Zing T. Beitrag zur schotteranalyse. Schweizerische Mineralogische und Petrologische Mitteilungen 1935;15:38–140.
[43] Neumann J, Simon J-W, Reese S. Digital sieving of irregular 3D particles—A study using XRCT and statistically similar synthetic data. Powder Technol 2018;338:1001–15.
[44] Jin Q, Zeng L, Chen X, Li P, Fu H, Zhou Y, et al. Portable digital holographic particle analyzer (DHPA) for pneumatically conveyed fuel monitoring: Design and validation. Powder Technol 2023;430:119030.
[45] Mathews JP, Eser S, Hatcher PG, Scaroni AW. The shape of pulverized bituminous vitrinite coal particles. Kona Powder Part J 2007;25:145–52.